PCCP

Accepted Manuscript

ROYAL SOCIETY OF CHEMISTRY

www.rsc.org/pccp

Journal Name

ARTICLE

Ultrafast Structural Flattening Motion in Photoinduced Excited State Dynamics of a Bis(dimine) Copper(I) Complex

Received 00th January 20xx,
Accepted 00th January 20xx

DOI: 10.1039/x0xx00000x

www.rsc.org/

Likai Du,[a,b,c] Zhenggang Lan*[a,b,c]

The ultrafast photoinduced structural change dynamics of a prototypical Cu(I) complex, namely, $[Cu(dmp)_2]^+$ (dmp = 2,9-dimethyl-1,10-phenanthroline), is investigated based on the theoretical analysis of static and dynamical calculations at all-atomic level. This work mainly focuses on the intriguing structural flattening feature of $[Cu(dmp)_2]^+$ occurring in the metal-to-ligand charge transfer singlet excited state (^{1}MLCT) on the sub-picosecond timescale. Our estimated time constant (~675fs) of this "flattening" motion is in good agreement with recent experimental values. The full-dimensional excited-state nonadiabatic dynamic simulation provides a direct view of the ultrafast photoinduced events of the $[Cu(dmp)_2]^+$, especially, the structural flattening mechanism on the S_1 state. Several molecular motions (such as Cu-N stretching, the motion of the substituted groups etc.) with distinguishable time scales are involved in the flattening dynamics. The Fourier transformation of the time-dependent oscillation of Cu-N bond and N-Cu-N bond angle provides consistent conclusions with the experimental spectrum analysis. These dynamics details imply that various nuclear motions are strongly coupled in the high-dimensional excited-state potential energy surface responsible for the geometrical evolution of $[Cu(dmp)_2]^+$. This work provides us a unique fundamental understanding of the ultrafast photoinduced excited-state nonadiabatic process of Cu(I) complexes and their derivatives, which should have potential impacts to various research fields, such as photo-catalysts, dye-sensitized solar cells (DSSCs), and organic light emitting diodes (OLEDs).

Introduction

The copper complexes, especially Cu(I), usually exhibit highly interesting and complicated excited state dynamics, such as metal-to-ligand charge transfer (MLCT) excitation in the visible range, the long-lifetime triplet MLCT states, and the photoinduced structural flattening[1-4]. As a group of photovoltaic materials alternative to the relatively expensive ruthenium(II) and osmium(II) complexes[5-10], the complexes based on more abundant Cu(I) have attracted much attentions due to their redox and luminescence properties potentially applicable for diverse applications[11-14], i.e. photocatalysts[15], dye-sensitized solar cells (DSSCs)[16], and organic light emitting diodes (OLEDs) materials[17]. Their possible extensive applications have become the main driving force for large research efforts aiming at understanding their fundamental photophysical and photochemical properties[18, 19].

Among them, several Bis(diimine) Cu(I) complexes have received significant attentions due to their visible absorption and long-lived emission of the metal-to-ligand charge transfer (MLCT) states[20], which are highly suitable for photosensitizers and photocatalysts. By the comparison with the well-known $[Ru(bpy)_3]^{2+}$ system[9, 21, 22], an interesting feature of the Cu(I) complexes is their photoinduced structural change, namely "flattening" dynamics on the excited states[23-26]. Upon excitation, a *d* electron of the central Cu(I) is transferred to the ligands, and the central copper is formally oxidized from Cu(I) to Cu(II). Therefore, the geometrical evolution of the Bis(diimine) Cu(I) complexes on the excited state is sometimes explained by the structural difference between tetrahedral Cu(I) complexes and square planar Cu(II) complexes. The former Cu(I) (d^{10}) mostly prefers the four-coordinated (tetrahedral) geometry, while the latter Cu(II) (d^9) prefers a six- (distorted octahedral) or five-coordinated (square pyramidal or trigonal bipyramidal) geometry[27, 28]. For example, the $[Cu(dmp)_2]^+$ (dmp = 2,9-dimethyl-1,10-phenanthroline) is a well-known prototypical Bis(diimine) Cu(I) complex (Fig. 1), which could undergo a large photoinduced structural flattening [20, 29-31].

[a] Key Laboratory of Biobased Materials, Qingdao Institute of Bioenergy and Bioprocess Technology, Chinese Academy of Sciences, Qingdao, 266101, Shandong, People's Republic of China. E-mail: lanzg@qibebt.ac.cn; Fax: +86-532-80662778; Tel: +86-532-80662630
[b] The Qingdao Key Lab of Solar Energy Utilization and Energy Storage Technology,Qingdao Institute of Bioenergy and Bioprocess Technology, Chinese Academy of Sciences, Qingdao, 266101, Shandong, People's Republic of China..
[c] University of Chinese Academy of Sciences, Beijing 100049, People's Republic of China.
Electronic Supplementary Information (ESI) available.
See DOI: 10.1039/x0xx00000x

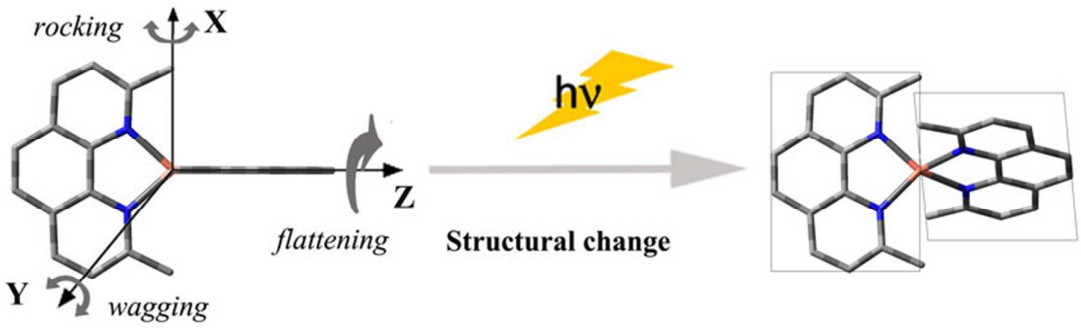

Fig. 1 Photoinduced structural flattening of the $[Cu(dmp)_2]^+$ in the ^{1}MLCT excited state. The hydrogen atoms were omitted for clarify. Possible motions between dmp ligands, namely wagging, rocking and flattening motions, were defined.

The photochemistry and photophysics of Bis(diimine) Cu(I) complexes are governed by various excited-state processes, including internal conversion (IC), structural flattening distortions, intersystem crossing (ISC), and etc. Due to their complicated ultrafast structural dynamics, a detailed understanding of these processes requires both state-of-art experimental observations and sophisticated theoretical studies. So for, the time-resolved spectroscopic investigations of $[Cu(dmp)_2]^+$ and its derivatives have been performed by a few groups[32-34, 20, 29, 30, 35-39]. Typically, early ultrafast excited states dynamics of $[Cu(dmp)_2]^+$ displays two time constants, one sub-picosecond (i.e. 660fs, 800fs) and one on the order of 10-20 ps[20, 39]. The sub-picosecond component was originally assigned to ISC in the early study of Chen et al., due to the structural similarities of $[Cu(dmp)_2]^+$ and $Ru(bpy)_3]^{2+}$, while the longer component was assigned to structural rearrangement .[33] A recent quantum wavepacket dynamics studies with multiconfigurational time-dependent Hartree (MCTDH) approach[40], based on a reduced model Hamiltonian, also highlighted the possible role of ISC at the Franck-Condon (FC) geometry. However, the assignment of the ISC process is still an open and controversial problem. For example, Nozaki and co-workers reported different assignments[34], in which ISC was assigned to the slower time component (10－20 ps). Later, Chen and co-workers[29] also reported a reversal of their previous assignments, and concluded that the ISC should occur on longer time scales, much slower than the initial structural distortion. Nowadays, several groups[34, 20, 29, 38, 31] usually assigned the shortest time component (a few hundred femoseconds) to IC and structural flattening, and the longer time component (10-20 ps) to ISC. Tahara and co-workers further demonstrate that the time scales of the structural flattening and the ISC in the lowest ^{1}MLCT state are clearly well-separated, with time constants of ~0.8 ps (structural change) and ~10 ps (ISC) for a few Bis(diimine) Cu(I) complexes.[30, 31] In the theoretical aspects, although a few uncertainty of the assignments [40], it is clear that the structural flatterning distortion largely weakens of spin-orbital couplings, further significantly slows down the ISC process of $[Cu(dmp)_2]^+$ as the structure distorts away from the ideal tetrahedral geometry[34, 29, 31].

Recent femtosecond time-resolved spectra demonstrated that the flattening distortion predominantly occurs in the ^{1}MLCT state on the sub-picosecond time scale, [30, 31] which is a typical character in a series of Cu(I) complexes. To address this issue, we focus on the early stage of photoinduced excited-state dynamics attributable to the ultrafast IC and the structural flattening distortion. Currently, the full-dimensional excited-state dynamics for the large transition metal complexes is still a great challenging topic. Here, the on-the-fly nonadiabatic surface hopping dynamics at the TDDFT level were performed to study the excited-state dynamics of the $[Cu(dmp)_2]^+$ complex. The on-the-fly scheme includes all nuclear degrees of freedom, which is very suitable to provide a rather illustrative picture of the large structural changes of the realistic $[Cu(dmp)_2]^+$ complex in the ^{1}MLCT excited state. Our calculations predicted the time constant of the "flattening" dynamics in good agreement with a series of recent experimental values.[20, 29, 30, 35, 38, 31] Our calculations also clearly identified the role of various electron-nuclei coupled motions involved in the structural flattering dynamics. This work is supposed to provide us some fundamental atomic-level insights on the excited state dynamics of the Bis(diimine) Cu(I) complex in the applications of photocatalysts, dye-sensitized solar cells (DSSCs), and organic light emitting diodes (OLEDs).

Methods

The minimum-energy geometries of the $[Cu(dmp)_2]^+$ complex for the ground state (S_0) were optimized at the DFT/6-31G* level with BHandHLYP, M06-2X, and CAM-B3LYP functionals. The low-lying singlet excited state geometries and properties were computed using the TDDFT method with a few functionals (BHandHLYP, M06-2X, and CAM-B3LYP). All optimizations were performed without any symmetry constraints. The vertical excitation energies, and simulated spectra were computed at the TDDFT/6-31G* level for a few low-lying excited excited states. For validation, our results at the DFT/TDDFT level were compared with available

experimental data. For the bis(diimine) Cu(I) complexes, the all electron basis sets were commonly used in recent theoretical investigations due to their good performance compared with experimental data[34, 37]. The similar approaches were also taken by a few of extensive benchmarking studies for the ground and excited properties of some copper complexes with various theoretical methods [41, 42]. Thus an all electron basis set 6-31G* basis set was employed here, because the computational cost is still acceptable in this model. Certainly, when the larger copper complexes are considered, the effective core potential of copper becomes a practical approach to speed up the electronic-structure calculations. All the above calculations were performed with Gaussian 09 package[43].

The ultrafast excited-state dynamics of the $[Cu(dmp)_2]^+$ complex was investigated by on-the-fly surface hopping approach. Here, we give a short description of the semiclassical trajectory surface hopping procedure[44, 45], especially, the on-the-fly dynamics, which have been adopted in the JADE package [46, 47]. In the surface hopping dynamics, the nuclear and electronic degrees of freedom are treated by classical and quantum dynamics, respectively. The motion of the nuclear degrees of freedom are represented by independent classical trajectories on the currently occupied electronic state, which is computed by the numerical integration of Newton's equations. The electronic motion is treated by the propagation of electronic wavefunction by solving time-dependent Schrödinger equation. At each time step, nonadiabatic transitions between excited states were taken into account via Tully's fewest switches approach[48]. Finally a large number of trajectories were computed to achieve the final statistical meaningful results. This approach is possible to treat relatively large and realistic molecular systems with full degree of freedom (DoF). Dynamics treatment with more accurate electronic-structure and advanced dynamical methods with full dimensionality should represent the great challenge for the future. The potential energies and nuclear gradients were computed by the TDDFT method. The numerical nonadiabatic couplings with respect to time[49, 45, 50, 51] were adopted in the nonadiabatic surface hopping dynamics as implemented in JADE package[46], since the analytic nonadiabatic couplings at the TDDFT level are still not commonly available in most of the standard QC packages. The decoherence correction proposed by Granucci et. al.[52] was taken and the parameter is set to α=0.1 Hartree. The time step for integration of classical equations was 0.5 fs and of quantum equations, 0.005 fs. The initial geometries and velocities of the excited state dynamics simulations were generated from the Wigner distribution function [53, 54] of the first vibrational level of the ground electronic state. The absorption spectrum was also calculated at TDDFT level by collecting the oscillation strength at the corresponding transition energy over a large number of sampled geometries. Starting from the initial sampling geometries of the ground state, the $[Cu(dmp)_2]^+$ complex is electronically excited to the S_n (S_2 or S_3) state, as reported in the experimental studies[33, 34, 20, 29, 30, 35, 38, 31]. And 78 trajectories starting from each state (S_2/S_3) were calculated. The CAM-B3LYP[55] and M06-2X[56] functionals were used in the TDDFT calculations. All calculations and data analysis were done within JADE package, interfaced with Gaussian 09 package. A few technical details in the trajectory analysis were summarized in the Supporting Information (SI).

Results and Discussions

The Structures and Properties of the $[Cu(dmp)_2]^+$ Complex

In Fig. 1, we show the optimized ground (S_0) and low-lying excited state (S_1) geometries of the $[Cu(dmp)_2]^+$. The optimized geometry at the S_0 state of $[Cu(dmp)_2]^+$ confirms the perpendicular orientation of the dmp ligands (D_{2d} symmetry) [3, 34, 20]. The lowest singlet excited state (S_1) of the $[Cu(dmp)_2]^+$ complex was optimized without any symmetry constraints. A significant geometric distortion between the ground and the excited state was observed (Fig. 1). The interligand dihedral angle (φ) was 70.4°at the S_1 minima. The details of the calculations of the interligand dihedral angle (φ) were given in SI. The critical geometric parameters with CAM-B3LYP, M06-2X and BHandHLYP functionals were also collected in Table S1. Interestingly, the Cu-N bond length for each ligand is split into two groups on the excited-state minima. Two Cu-N bonds associated with one ligand become shorter, while the other two Cu-N bonds become longer. This indicates that the geometries of two ligands become not fully equivalent at the S_1 minima. The geometry evolution on the excited state should be attributed to different electronic transitions at the perpendicular and flattened geometry (Fig. S1). At the perpendicular geometry, the LUMO orbital is delocalized over both dmp ligands. Meanwhile, at the flattened geometry, the LUMO orbital is localized on one dmp ligand, and the excitation was from the copper ion (HOMO) to one of the dmp ligand (LUMO). This asymmetrical excitation also explains the slight geometrical difference of two ligands at the S_1 minima.

Journal Name

ARTICLE

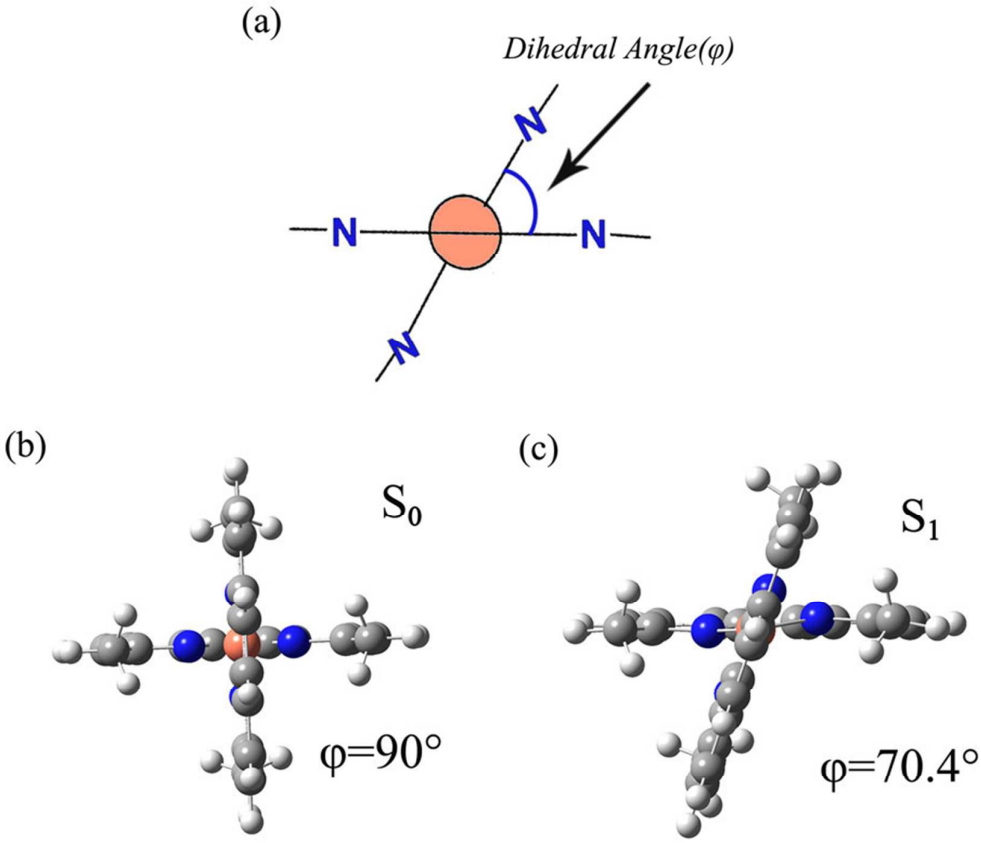

Fig. 2 (a) The definition of interligand dihedral angle (φ) between dmp ligands; and the optimized structures of the $[Cu(dmp)_2]^+$ complex at CAM-B3LYP level for (b) the ground state (S_0); (c) the low-lying S_1 excited state.

We then analyzed the nature of low-lying singlet excited states with the transition density analysis approach[57-60]. Two blocks (the copper ion and dmp ligands) were used to build intra-unit and inter-unit transition probabilities. It is clear that the low-lying excited states (S_1, S_2, and S_3) are typically MLCT states (Fig. S2). Table 1 lists the calculated and experimental excitation energies. For $[Cu(dmp)_2]^+$, the experimental assignment of the ^{1}MLCT absorption peaks are about 2.71 eV ($S_0 \rightarrow S_n$, n=2 or 3) with a weaker shoulder at 2.31 eV ($S_0 \rightarrow S_1$). [38] The excitation energy from S_0 to S_n is relatively higher for BHandHLYP and M06-2X functionals, while the CAM-B3LYP functional seems to improve the prediction of the $S_0 \rightarrow S_n$ excitation energy. The better performance of CAM-B3LYP functional[55] could be rationalized by its improvement on the charge transfer states (S_1, S_2, and S_3) in the description of the $[Cu(dmp)_2]^+$ complex. However, a perfect agreement between theory and experiment should not be expected, since absorption spectra are measured in solvent. The difference between theoretical and experimental results is largely reduced, when our calculations took both the $[Cu(dmp)_2]^+$ cation and its counterpart anion (PF_6^-) into account. After the inclusion of its counterpart anions (i.e. PF_6^-), the $S_0 \rightarrow S_1$ excitation energy (~2.43 eV) was comparable to the experimental one (~2.31 eV). Note that the incorporation of the solvent effect (in dichloromethane) only shows minor contribution. This excitation energy dependence on the existent of the PF_6^- anion may be partially caused by the structural distortion effects (φ=85.9°, in Fig. S3), which is consist with X-ray crystallographic data (φ=68°~88°) on $[Cu(dmp)_2]^+$ complex with various counterpart anions[23, 61, 2, 62] The excitation energy would be lowered by ~0.1 eV along with the decreasing of the

interligand dihedral angle (Fig. 3a). And the present of the anion may also stabilize the MLCT excited state species and lower the excitation energies. Further transition density analysis of $[Cu(dmp)_2](PF_6^-)$ complex confirms that the low-lying excited states (S_1, S_2, and S_3) are still typically MLCT states (Fig. S4). The anion effects show minor contribution to the shift of the absorption peak (Fig. S5). Although the existence of the anion has little effect on the position of the main absorption, the anion slightly changes the relative intensity of the shoulder compared to the absorption spectra of the $[Cu(dmp)_2]^+$. On the basis of a few experimental reports [23, 24, 63], the weak shoulder is attributed to the weak absorption of the first singlet MLCT transition for the geometries with slightly flattened pseudotetrahedral structure. Overall, the result of CAM-B3LYP functional is reasonable in our studies of the $[Cu(dmp)_2]^+$ complex.

Table 1. The calculated and experimental excitation energies (eV) of the $[Cu(dmp)_2]^+$ and $[Cu(dmp)_2](PF_6)$ complex. The effect of the dichloromethane solution was taken into account with a single point calculation at the TDDFT/CAM-B3LYP level with PCM model (in the bracket).

Species	$[Cu(dmp)_2]^+$			$[Cu(dmp)_2](PF_6)$	
	BHandHLYP	M06-2X	CAM-B3LYP	CAM-B3LYP	exp.[a]
S_1	3.11	3.03	2.62	2.43 (2.47)	2.31
S_2	3.20	3.14	2.73	2.57 (2.60)	2.71
S_3	3.42	3.39	2.94	2.96 (2.98)	

[a] values are taken from ref. 38.

The photoinduced structural flattening is an important feature of the $Cu[(dmp)_2]^+$ complex. Herein, we performed an PES analysis along the interligand dihedral angle (φ, see Fig. 2) for the low-lying singlet excited states. The geometries were relaxed on the ground state along this interligand dihedral angle. As shown in Fig. 3a, the topology of the PES for S_1 and S_2 states are relatively flat at or near tetrahedral geometry (FC region with φ=90º). Furthermore, the excitation energy of the S_1 state is lowered when the $Cu[(dmp)_2]^+$ complex distorts away from its tetrahedral geometry. In order to get more insight on the geometric dependent of ^{1}MLCT states, the transition density corresponding to the metal-to-ligand charge-transfer component is shown in Fig. 3b as a function of the interligand dihedral angle. For the S_1 state, the charge transfer between metal and ligands is only weakly dependent on the interligand angle. Meanwhile, the dependence of S_2 and S_2 state becomes more visible.

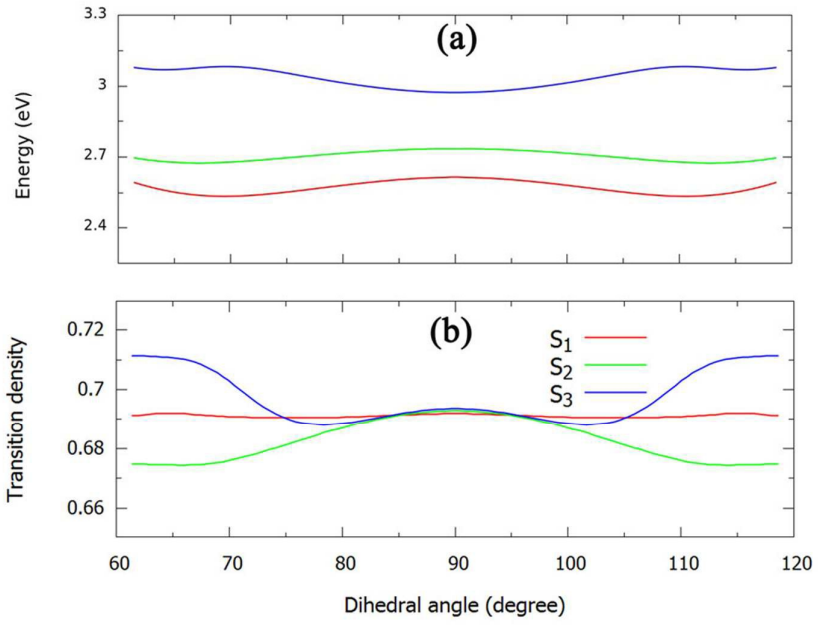

Fig. 3 (a) The potential energy curves of S_1, S_2, and S_3 states, as a function of interligand dihedral angle (φ). (b) the transition density amplitude of the metal-to-ligand charge-transfer component for S_1, S_2, and S_3 states as a function of interligand dihedral angle (φ), which can be used to measure the contribution of the charge-transfer component for each state.

Journal Name

ARTICLE

Photoinduced Excited State Dynamics of the $[Cu(dmp)_2]^+$ Complex

Here, we try to investigate the early-stage ultrafast dynamics on the coupled low-lying singlet surface, and its subsequent structural flattening on the S_1 state. The experimental works usually study the excited-state dynamics starting from the higher S_n (S_2 or S_3) state [38, 31]. Thus, we begin our ultrafast nonadiabatic dynamics simulation from the S_n state. Previous experimental studies proposed that, after the $[Cu(dmp)_2]^+$ is excited in to the S_n state, the excited state decay process is composed of several processes with distinguishable time scales, namely the ultrafast IC to the S_1 state, the structural flattening distortion on the S_1 state, and the subsequent ISC process around 10-20 ps. [20, 29, 30, 35, 64, 38, 31]

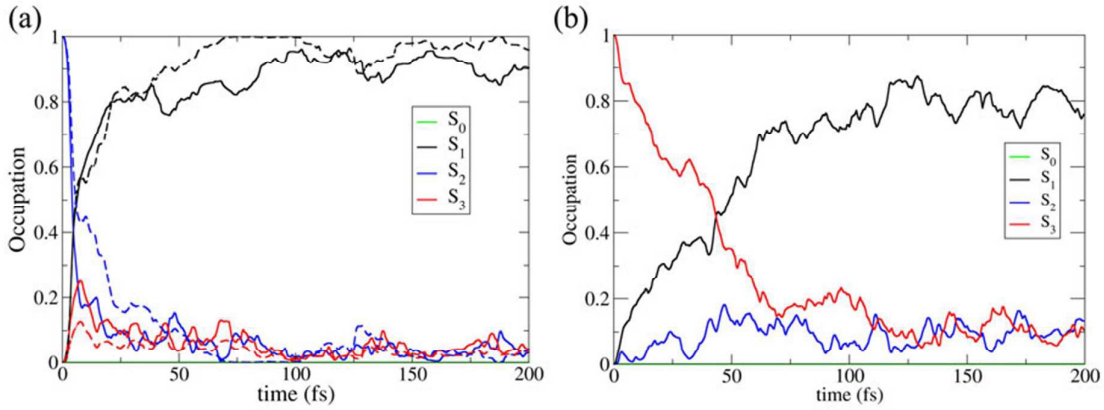

Fig. 4 (a) The average fractional occupation of trajectories for each state starting at S_2 state, and the dashed line was calculated at M06-2X level; (b) the average fractional occupation of trajectories for each state starting at S_3 state.

The Initial Ultrafast Nonadiabatic Dynamics

Fig. 4a shows the average fraction of trajectories for each state, after excited into S_2 state. For $[Cu(dmp)_2]^+$, the initial quick drop of the S_2 population is observed within first ~30 fs. And then, the continuous decay of the S_2 state takes place from 20% to 5% along with fast oscillations. Later, the S_2 population is kept below 10% beyond 100 fs. This ultrafast decay of the S_2 state is relatively faster than the experimental data (τ = 47 fs) [31]. This is expected, due to the ignorance of the hindrance effects of solvent molecules, the missing of the anion or the lackness of the possible contribution from the minor ISC channels. The S_1 population increases to more than 90% beyond 100 fs. In Fig. 4a, the S_3 state shows a low probability in the initial stage of the trajectories, which can be rationalized by the PES profile of the S_3 state (Fig. 3a). At the FC geometry, the energy gap between S_2 and S_3 is smaller. In addition, it may also become closer during the trajectory propagation (Fig. S6). We also tried to examine the dependence of the excited-state decay on DFT functionals. Compared with CAM-B3LYP results, the M06-2X functional predicts the similar ultrafast decay behavior, although slightly slower decay of the S_2 state is observed.

Finally, the excited state dynamics from the S_3 state was also considered (Fig. 3b). The decay to the S_1 state takes place with the time constant about 50 fs, which is similar to the recent experimental assignment of initial IC process to the S1 state[31]. Although the ground electronic state (S_0) was also included in the current surface hopping dynamics, we do not see any trajectory jumping to the S_0 within the simulation time scale (Fig. S7, S8). Overall, no matter which state the trajectories start from, after the quick drop of fractional occupation of the initial state (S_n), the system stays on the S_1 PES. Overall, the subsequent excited state dynamic behavior is quite similar. And thus we would perform further trajectory analysis based on the simulation (TDDFT/CAM-B3LYP level) starting from S_2 state in the following discussions.

Journal Name

ARTICLE

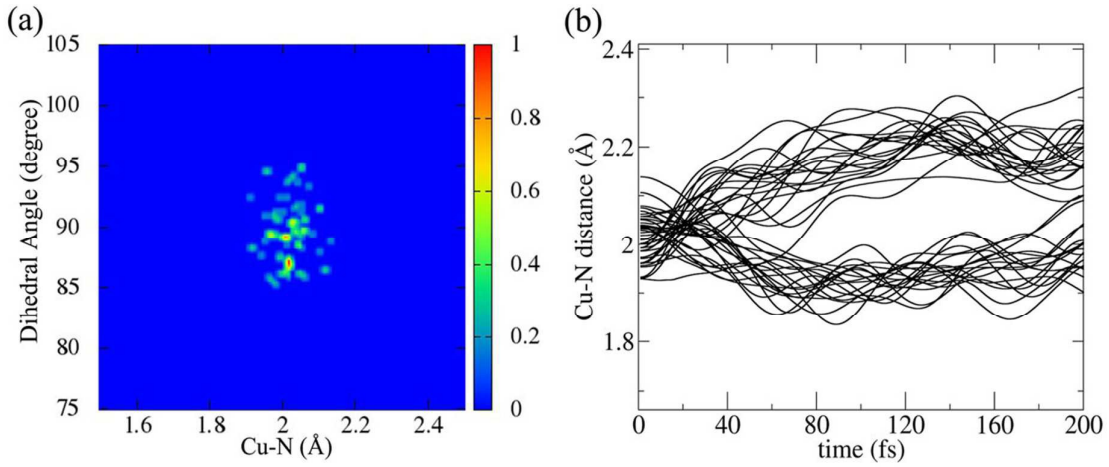

Fig. 5 (a) Two dimensional geometric distribution of the Cu-N distance and interligand dihedral angle (φ) for the $S_n \rightarrow S_1$ hopping structures; (b) the Cu-N bond stretching of $[Cu(dmp)_2]^+$ as a function of time (fs).

Next, the distribution of the Cu-N distance and interligand dihedral angle (φ) was analyzed during the $S_n \rightarrow S_1$ hopping events. Fig. 5a indicates that nearly perpendicular geometries are preferred at the avoided crossing points (S_n/S_1); however, the slightly distorted geometries are also possible. Generally, the hopping geometries retain similar as the initial FC geometry at the S_0 state. During the ultrafast IC dynamics from the S_n to the S_1 state, the significant Cu-N stretching motion was observed, which mainly splits into two branches (Fig. 5b). This can be rationalized by the following fact. When the system moves away from the FC geometry, the S_1 state displays the electronic character corresponding to the MLCT transition of a single electron from the copper ion (HOMO) to one of the dmp ligands (LUMO) (Fig. S1). This electrostatic interaction between the copper ion and ligands may induce a sudden force to drive the Cu-N stretching motion. The asymmetrical electronic excitation should induce different force for the Cu-N bonds on two ligands, resulting in the splitting feature in Fig 5b. After this, the structural flattening distortion begins to occur on the S_1 state with longer time-scale dynamics.

The S_1 State Structural Flattening Dynamics

In the following discussion, we focus on the structural flattening dynamics on the S_1 PES within one picosecond. Recent experimental studies reveal that the timescales of the successive structural change and ISC process seems to be well-separated, occurring with time constants of ~600-800 fs and ~10-20 ps. [30, 36] Based on these experimental observations, the ISCs into the triplet states should be rare within the sub-picosecond timescale. Instead, the ISC process may occur on the time scale of ~10 ps, which is beyond our on-the-fly surface hopping dynamic simulation. Therefore, we pay our attention on the early-stage dynamics, especially, the unique structural flattening in the S_1 state for various Cu(I) complexes, which is supposed to be the major contribution (~70%)[20] within the subpicosecond time scale.

Journal Name

ARTICLE

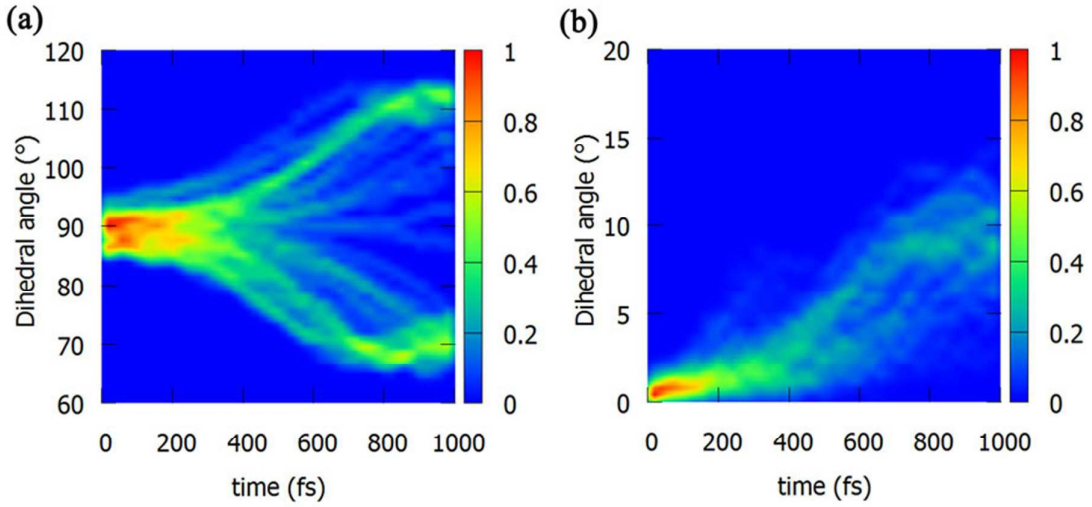

Fig. 6 (a) Time evolution of the interligand dihedral angle (φ); (b) The dihedral angle of one dmp ligand with respect to its initial frame, as a function of time.

The time evolution of the distribution of the interligand dihedral angle (φ) was shown in Fig. 6a. We also provided time evolution of the interligand dihedral angle for several specific trajectories (Figure S9). Initially, the structural flattening motion is minor within the first 200 fs. Then the structural flattening angle begins to appear, and becomes stable around 600-750 fs. If we take the middle value as the structural flattening time constant (~675 fs), this agrees well with experimental assignment of time constants of the structural flattening distortion within 1000fs[20, 30, 37-39, 31], i.e. 660fs[20] or 800fs[30, 39]. Furthermore, the current calculations clearly show that the IC dynamics to the S_1 state (<100 fs) and the beginning of structural flattening motion on the S_1 state (~200 fs) are indeed well-separated, as suggested by a series of recent experimental studies [30, 36, 31]. Note that the interligand dihedral angle (φ) becomes stable until about 70º or 110º, which is very close to our optimized geometry of S_1 state (φ=70.4º, Fig. 2). Additionally, the trajectories mainly split into two branches in terms of the directional behavior during the structural flattening dynamics. The clockwise and anti-clockwise flattening motions are nearly identical, while different ratios for each branch may be expected if this symmetric character is destroyed, i.e. by the inclusion of its counterpart anion or asymmetric substitutes. We also tried to monitor the motion of each dmp ligand with respect to its initial frame (see SI), as a function of time (Fig. 6b). For a specific trajectory, the rotation of one dmp ligand may range from less than 5º to as large as 15º (Fig. S9). On average, each dmp ligand rotates about 10º to complete this structural flattening distortion.

Journal Name

ARTICLE

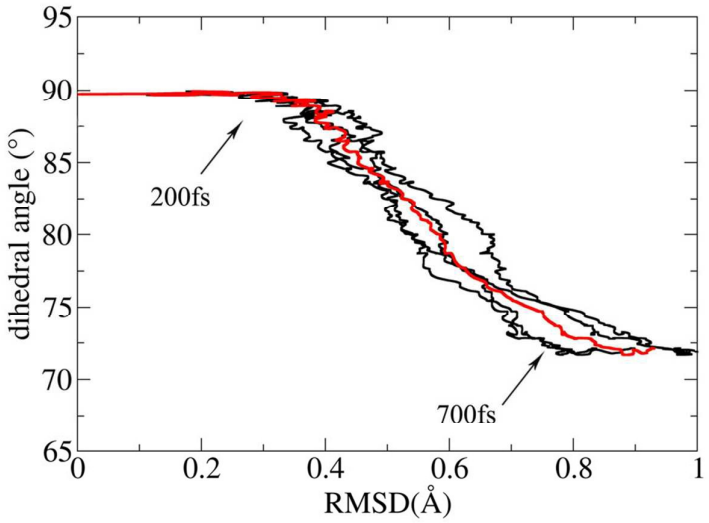

Fig. 7 The correlation between the motion of methyl groups (-CH_3) and the interligand dihedral angle (φ), which is averaged over all trajectories. The black lines refer to four methyl groups, while the red line refers to their average values. Note only the branch with dihedral angle below 90° was shown, due to its symmetric character.

Another interesting feature of the Bis(diimine) Cu(I) complexes is their cooperatively steric hindrance influence of the substitutes effects at the 2,9-positions of 1,10-phenanthroline, which can dramatically influence the excited state characteristics and dynamics. [65, 38, 39, 31, 66] Here, the root-mean-square deviation (RMSD) is used to monitor the motion of the methyl group (-CH_3) with respect to its initial structure along the trajectories. We also analyzed the correlation between the relaxation of methyl group and the evolution of the interligand flattening angle (φ). Our results indicate the structural flattening process takes place in a stepwise manner (Fig. 7). Within the first ~ 200 fs, the relaxation of four methyl groups starts prior to the structural flattening dynamics, which is obviously reflected by the increasing RMSD values, in contrast to nearly constant interligand dihedral angle (φ). Later, the dihedral angle (φ) begins to increase along with the relaxation of methyl groups. After ~700 fs, the dihedral angle keeps stable (φ≈70°), while the methyl groups undergo further relaxation. Therefore, the active motion of the substituted groups should be considered to achieve the proper topographic description of the excited state PES. This feature also implies that the different substituted moieties attached in the ligand may have potential influences on the geometrical evolution dynamics for Bis(diimine) Cu(I) complexes. A few recent experiments have been reported to utilize the substitute effects to improve the performance of copper(I)-based dye sensitized solar cells. [17, 35, 64, 38, 18, 66]

Journal Name

ARTICLE

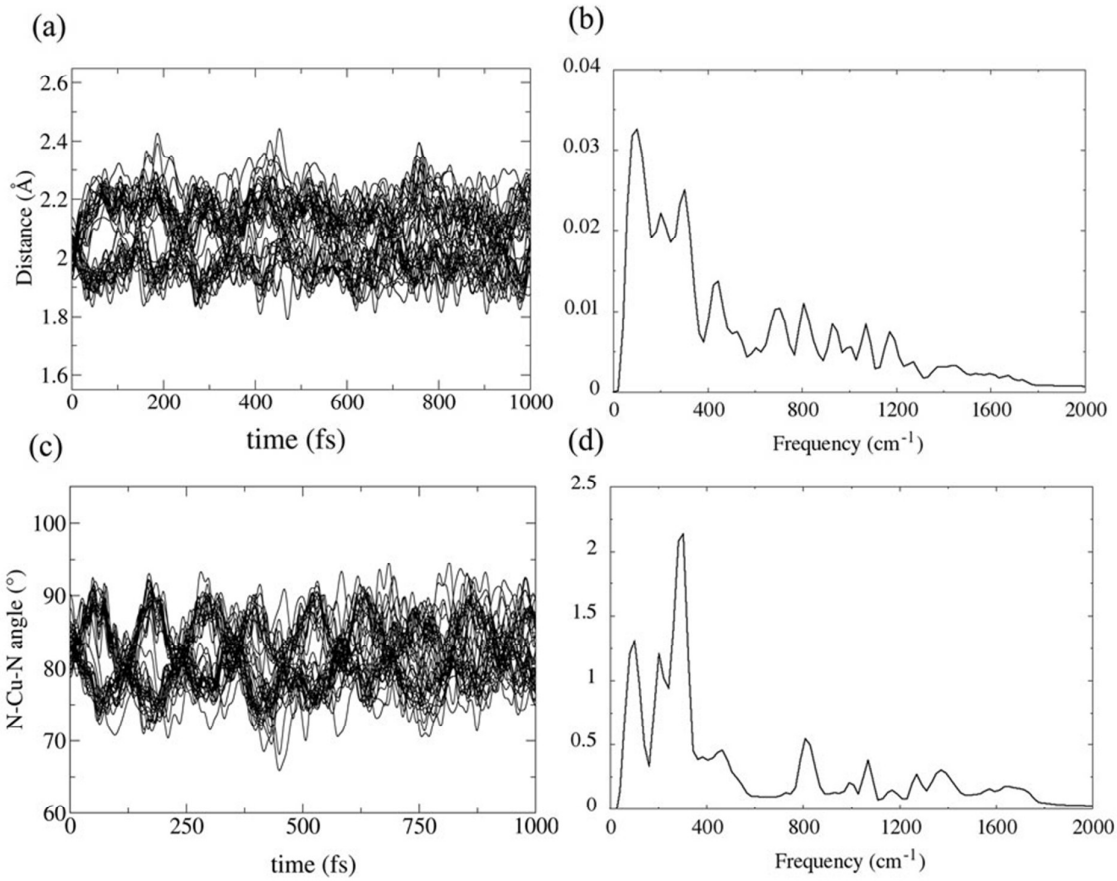

Fig. 8 Time evolution of the Cu-N bond length (a) and the N-Cu-N bond angle (b); the Fourier transformation of the Cu-N bond length (c) and the N-Cu-N bond angle (d). The zero component of the Fourier transform has been truncated for illustrative purposes.

Finally, we pay our attention to the time evolution of several critical geometric parameters. Significant fluctuations of the Cu-N bond length and N-Cu-N bond angle were observed (Fig. 8), which implies the collective nuclear motion on the S_1 state[31]. Fig. 8 also shows the Fourier transformation of the oscillation of the Cu-N bond length and N-Cu-N bond angle. Due to the limited simulation timescale, the resolution of the Fourier transformation may not provide a very explicit assignment. However, we may provide an rough assignment of the several important frequency domains of vibrational motions on the basis of recent spectroscopic and theoretical studies [30, 40]. For instance, the vibration (~150 cm^{-1}) with the largest contribution (Fig. 8b) is very close to the largest contribution (125 cm^{-1}) in the Fourier transformation of the oscillation in the transient absorption signal[30]. Tahara and co-workers have assigned this vibration to the "breathing" motion of the complex, i.e. the collective oscillation of Cu-N bond. Note that this vibration is related to the oscillation with the period of ~300 fs , which can be easily identified in Fig. 8a as well. The vibrations around 200~300 cm^{-1} could be assigned to the rocking motions. The smaller peak around 430 cm^{-1} is related to the bending motion involving the N-Cu-N bond angle. The vibrations with higher frequency (~800 cm^{-1}) could be attributed to the vibrations containing Cu-N stretching motion. All of these modes are also consistent with the important mode assignments of Capano et. al[31].

The geometrical flexibility of the dmp ligands was also investigated to rationalize the dynamical details in the structural flattening motion. The out-of-plane motion of a dmp ligand is described by the residue with respect to the planar equation (Fig. S10a in SI). During the trajectory propagation, the deviation

from an ideal plane was less than 0.1Å per atom, which is less than 10 % of a typical C-C bond length. The wagging and rocking (Scheme 1) vibrations cause very small structural fluctuations ~3° (Fig. S10b), in contrast to ~20° for the structural flattening motion. Therefore, the structural flattening motion is dominated in the dynamics, although the other nuclear motion is also involved in realistic dynamic processes. In addition, significant periodic motions (~300 fs) were also observed in the wagging and rocking motions, which were assigned as the "breathing" motion. Thus, such collective oscillation of Cu-N bond should be a typical character in the structural flatterning dynamics of the $[Cu(dmp)_2]^+$ complex.

Table 2. Time constants (ps) of several critical mechanistic process obtained from excited state dynamics simulation, and recent experimental conclusions of the low-lying excited states of the $[Cu(dmp)_2]^+$ complex.

	This work	ref 33	ref 34	ref 29	ref 20,30	ref 38
$S_3 \rightarrow S_2$ and S_1	0.03-0.05	–	–	0.08	0.045	–
$S_1^{perpendicular} \rightarrow S_1^{flattened}$	0.60-0.75	10-20	–	0.34-0.70	0.66-0.80	< 1.0
Singlet to triplet ISC[a]	–	0.5-0.7	~15	10-15	7.40-10.0	10-20

[a] The current work does not address the ISC process.

Conclusions

The Bis(dimine) Cu(I) complexes, such as $[Cu(dmp)_2]^+$, have received great research interests, because their photophysical characteristics are highly suitable for photosensitizers and photocatalysts. Here, we performed a detail investigation of the initially photoinduced excited state dynamics of the $[Cu(dmp)_2]^+$ involving the ultrafast IC (S_n/S_1) and the structural flattening process occurring on the S_1 state, which is an intriguing feature of these Cu(I) complexes. The full dimensional excited-state dynamics of transition metal complex are still challenging due to the large number of the degree of freedom. Thus, the on-the-fly nonadiabatic surface hopping dynamics was employed to study this electron-nuclei coupled relaxation dynamics at the sub-picosecond timescale, which provides us an direct view of ultrafast photoinduced process of the $[Cu(dmp)_2]^+$, especially, the structural flattening mechanism on the S_1 state.

Our excited state dynamic studies reveal that the photoinduced structural flattening process is composed of several events with distinguishable time scales (Table 1). At the early stage of the excited state dynamics of the $[Cu(dmp)_2]^+$ complex, the system undergoes an ultrafast internal conversion to the S_1 state. In this very short timescale (<200fs), significant motions of the Cu-N bond length and N-Cu-N bond angle are also observed. Later, the structural flattening process on the S_1 state begins to appear after ~200-300 fs, along with the relaxation of methyl groups. Note that the cooperative relaxation of methyl groups starts prior to the structural flattening dynamics, which should be important to avoid the steric hindrance of the substitutes. The interligand flattening angle (φ) becomes stable around 600-750 fs, and we take the middle value as the structural flattening time constant (~675 fs), which agrees well with a series of recent experimental values [20, 29, 30, 36, 38, 31]. Fourier transformations of the oscillation of the Cu-N bond length and N-Cu-N bond angle also identify several most important vibrational frequency domains, which are consistent to the recent theoretical and experimental assignments[30, 40]. At the same time, the planarity of two dmp ligands basically remains during the whole flattening dynamics.

Overall, the static and dynamic excited state calculations provide an illustrative picture of the photoinduced structural change in the ^{1}MLCT state. Since such a photoinduced structural change is an essential component in photophysics and photochemistry of the Cu(I) complexes, this detailed understanding of the ultrafast excited-state process is indispensable to the future development of the Cu(I)-based photovaltic materials as an alternative to the ruthenium(II) complexes. Finally, the full dimensional excited-state dynamics simulation of large transition metal complex is a challenging topic in the theoretical aspects. Further progress is also going on to consider a few important issues in the structural flattening dynamics, for example the anion/solvent effects, and the possible ISC contribution.

Acknowledgements

This work is supported by the CAS 100 Talent Project, and NSFC project (Grant Nos. 91233106, 21503249, and 21543008). This work was also supported by the Natural Science Foundation of Shandong Province for Distinguished Young Scholars (JQ201103). The authors thank the support by Natural Science Foundation of Shandong Province for Young Scientist (ZR2015BQ010). The authors also thank Supercomputing Centre, Computer Network Information Center, CAS and the Super Computational Centre of CAS-QIBEBT for providing computational resources.

.

Notes and references

1. J. A. Paulson, D. A. Krost, G. L. McPherson, R. D. Rogers and J. L. Atwood, *Inorg. Chem.*, 1980, **19**, 2519-2525.
2. C. T. Cunningham, J. J. Moore, K. L. H. Cunningham, P. E. Fanwick and D. R. McMillin, *Inorg. Chem.*, 2000, **39**, 3638-3644.
3. D. V. Scaltrito, D. W. Thompson, J. A. O'Callaghan and G. J. Meyer, *Coord. Chem. Rev.*, 2000, **208**, 243-266.
4. M. W. Mara, K. A. Fransted and L. X. Chen, *Coord. Chem. Rev.*, 2015, **282–283**, 2-18.

5. J. A. Simon, S. L. Curry, R. H. Schmehl, T. R. Schatz, P. Piotrowiak, X. Jin and R. P. Thummel, *J. Am. Chem. Soc.*, 1997, **119**, 11012-11022.
6. A. El-ghayoury, A. Harriman and R. Ziessel, *Chem. Commun.*, 1999, DOI: 10.1039/A905979B, 2027-2028.
7. A. Adronov and J. M. J. Frechet, *Chem. Commun.*, 2000, DOI: 10.1039/B005993P, 1701-1710.
8. D. S. Tyson, K. B. Henbest, J. Bialecki and F. N. Castellano, *J. Phys. Chem. A*, 2001, **105**, 8154-8161.
9. J. K. McCusker, *Acc. Chem. Res.*, 2003, **36**, 876-887.
10. R. Passalacqua, F. Loiseau, S. Campagna, Y.-Q. Fang and G. S. Hanan, *Angew. Chem., Int. Ed.*, 2003, **42**, 1608-1611.
11. M. T. Miller, P. K. Gantzel and T. B. Karpishin, *Angew. Chem., Int. Ed.*, 1998, **37**, 1556-1558.
12. M. Ruthkosky, C. A. Kelly, F. N. Castellano and G. J. Meyer, *Coord. Chem. Rev.*, 1998, **171**, 309-322.
13. M. T. Miller, P. K. Gantzel and T. B. Karpishin, *J. Am. Chem. Soc.*, 1999, **121**, 4292-4293.
14. D. G. Cuttell, S.-M. Kuang, P. E. Fanwick, D. R. McMillin and R. A. Walton, *J. Am. Chem. Soc.*, 2002, **124**, 6-7.
15. B. Kumar, M. Llorente, J. Froehlich, T. Dang, A. Sathrum and C. P. Kubiak, *Annu. Rev. Phys. Chem.*, 2012, **63**, 541-569.
16. M. Grätzel, *J. Photoch. Photobio. C*, 2003, **4**, 145-153.
17. E. Holder, B. M. W. Langeveld and U. S. Schubert, *Adv. Mater.*, 2005, **17**, 1109-1121.
18. C. E. Housecroft and E. C. Constable, *Chem. Soc. Rev.*, 2015, DOI: 10.1039/C5CS00215J.
19. M. W. Mara, D. N. Bowman, O. Buyukcakir, M. L. Shelby, K. Haldrup, J. Huang, M. R. Harpham, A. B. Stickrath, X. Zhang, J. F. Stoddart, A. Coskun, E. Jakubikova and L. X. Chen, *J. Am. Chem. Soc.*, 2015, **137**, 9670-9684.
20. M. Iwamura, S. Takeuchi and T. Tahara, *J. Am. Chem. Soc.*, 2007, **129**, 5248-5256.
21. C. E. McCusker and J. K. McCusker, *Inorg. Chem.*, 2011, **50**, 1656-1669.
22. A. M. Brown, C. E. McCusker and J. K. McCusker, *Dalton Trans.*, 2014, **43**, 17635-17646.
23. W. L. Parker and G. A. Crosby, *J. Phys. Chem.*, 1989, **93**, 5692-5696.
24. R. M. Everly and D. R. McMillin, *J. Phys. Chem.*, 1991, **95**, 9071-9075.
25. R. M. Everly, R. Ziessel, J. Suffert and D. R. McMillin, *Inorg. Chem.*, 1991, **30**, 559-561.
26. S. Sakaki, H. Mizutani and Y. Kase, *Inorg. Chem.*, 1992, **31**, 4575-4581.
27. B. J. Hathaway and D. E. Billing, *Coord. Chem. Rev.*, 1970, **5**, 143-207.
28. B. J. Hathaway, *Coord. Chem. Rev.*, 1981, **35**, 211-252.
29. G. B. Shaw, C. D. Grant, H. Shirota, E. W. Castner, G. J. Meyer and L. X. Chen, *J. Am. Chem. Soc.*, 2007, **129**, 2147-2160.
30. M. Iwamura, H. Watanabe, K. Ishii, S. Takeuchi and T. Tahara, *J. Am. Chem. Soc.*, 2011, **133**, 7728-7736.
31. M. Iwamura, S. Takeuchi and T. Tahara, *Acc. Chem. Res.*, 2015, **48**, 782-791.
32. L. X. Chen, G. Jennings, T. Liu, D. J. Gosztola, J. P. Hessler, D. V. Scaltrito and G. J. Meyer, *J. Am. Chem. Soc.*, 2002, **124**, 10861-10867.
33. L. X. Chen, G. B. Shaw, I. Novozhilova, T. Liu, G. Jennings, K. Attenkofer, G. J. Meyer and P. Coppens, *J. Am. Chem. Soc.*, 2003, **125**, 7022-7034.
34. Z. A. Siddique, Y. Yamamoto, T. Ohno and K. Nozaki, *Inorg. Chem.*, 2003, **42**, 6366-6378.
35. C. E. McCusker and F. N. Castellano, *Inorg. Chem.*, 2013, **52**, 8114-8120.
36. M. Iwamura, S. Takeuchi and T. Tahara, *Phys. Chem. Chem. Phys.*, 2014, **16**, 4143-4154.
37. G. Capano, U. Rothlisberger, I. Tavernelli and T. J. Penfold, *J. Phys. Chem. A*, 2015, **119**, 7026-7037.
38. S. Garakyaraghi, E. O. Danilov, C. E. McCusker and F. N. Castellano, *J. Phys. Chem. A*, 2015, **119**, 3181-3193.
39. L. Hua, M. Iwamura, S. Takeuchi and T. Tahara, *Phys. Chem. Chem. Phys.*, 2015, **17**, 2067-2077.
40. G. Capano, M. Chergui, U. Rothlisberger, I. Tavernelli and T. J. Penfold, *J. Phys. Chem. A*, 2014, **118**, 9861-9869.
41. A. Hoffmann, M. Rohrmüller, A. Jesser, I. dos Santos Vieira, W. G. Schmidt and S. Herres-Pawlis, *J. Comput. Chem.*, 2014, **35**, 2146-2161.
42. A. Jesser, M. Rohrmüller, W. G. Schmidt and S. Herres-Pawlis, *J. Comput. Chem.*, 2014, **35**, 1-17.
43. M. J. Frisch, G. W. Trucks, H. B. Schlegel, G. E. Scuseria, M. A. Robb, J. R. Cheeseman, G. Scalmani, V. Barone, B. Mennucci, G. A. Petersson, H. Nakatsuji, M. Caricato, X. Li, H. P. Hratchian, A. F. Izmaylov, J. Bloino, G. Zheng, J. L. Sonnenberg, M. Hada, M. Ehara, K. Toyota, R. Fukuda, J. Hasegawa, M. Ishida, T. Nakajima, Y. Honda, O. Kitao, H. Nakai, T. Vreven, J. A. Montgomery Jr., J. E. Peralta, F. Ogliaro, M. J. Bearpark, J. Heyd, E. N. Brothers, K. N. Kudin, V. N. Staroverov, R. Kobayashi, J. Normand, K. Raghavachari, A. P. Rendell, J. C. Burant, S. S. Iyengar, J. Tomasi, M. Cossi, N. Rega, N. J. Millam, M. Klene, J. E. Knox, J. B. Cross, V. Bakken, C. Adamo, J. Jaramillo, R. Gomperts, R. E. Stratmann, O. Yazyev, A. J. Austin, R. Cammi, C. Pomelli, J. W. Ochterski, R. L. Martin, K. Morokuma, V. G. Zakrzewski, G. A. Voth, P. Salvador, J. J. Dannenberg, S. Dapprich, A. D. Daniels, Ö. Farkas, J. B. Foresman, J. V. Ortiz, J. Cioslowski and D. J. Fox, *Journal*, 2009.
44. M. Barbatti, G. Granucci, M. Persico, M. Ruckenbauer, M. Vazdar, M. Eckert-Maksić and H. Lischka, *J. Photoch. Photobio. A.*, 2007, **190**, 228-240.
45. E. Tapavicza, I. Tavernelli and U. Rothlisberger, *Phys. Rev. Lett.*, 2007, **98**, 023001.
46. L. Du and Z. Lan, *J. Chem. Theory Comput.*, 2015, **11**, 1360-1374.
47. L. Du and Z. Lan, *J. Chem. Theory Comput.*, 2015, **11**, 4522-4523.
48. J. C. Tully, *J. Chem. Phys.*, 1990, **93**, 1061-1071.
49. H. Lischka, M. Dallos and R. Shepard, *Mol. Phys.*, 2002, **100**, 1647-1658.
50. U. Werner, R. Mitrić, T. Suzuki and V. Bonačić-Koutecký, *Chem. Phys.*, 2008, **349**, 319-324.
51. I. Tavernelli, E. Tapavicza and U. Rothlisberger, *J Mol. Struc.-Theochem*, 2009, **914**, 22-29.
52. G. Granucci, M. Persico and A. Zoccante, *J. Chem. Phys.*, 2010, **133**, 134111.
53. E. Wigner, *Phys. Rev.*, 1932, **40**, 749-759.
54. D. Sels and F. Brosens, *Physical Review E*, 2013, **88**, 042101.
55. T. Yanai, D. P. Tew and N. C. Handy, *Chem. Phys. Lett.*, 2004, **393**, 51-57.
56. Y. Zhao and D. Truhlar, *Theor. Chem. Acc.*, 2008, **120**, 215-241.
57. F. Plasser and H. Lischka, *J. Chem. Theory Comput.*, 2012, **8**, 2777-2789.
58. F. Plasser, S. A. Bäppler, M. Wormit and A. Dreuw, *J. Chem. Phys.*, 2014, **141**, 024107.
59. F. Plasser, M. Wormit and A. Dreuw, *J. Chem. Phys.*, 2014, **141**, 024106.
60. J. Huang, L. Du, D. Hu and Z. Lan, *J. Comput. Chem.*, 2015, **36**, 1858-1858.
61. A. J. Blake, S. J. Hill, P. Hubberstey and W.-S. Li, *J. Chem. Soc., Dalton Trans.*, 1998, DOI: 10.1039/A708796I, 909-916.
62. W. T. Eckenhoff and T. Pintauer, *Acta Crystallogr. E*, 2007, **63**, m800-m802.
63. K. A. Fransted, N. E. Jackson, R. Zong, M. W. Mara, J. Huang, M. R. Harpham, M. L. Shelby, R. P. Thummel and L. X. Chen, *J. Phys. Chem. A*, 2014, **118**, 10497-10506.
64. M. Chergui, *Acc. Chem. Res.*, 2015, **48**, 801-808.
65. M. K. Eggleston, D. R. McMillin, K. S. Koenig and A. J. Pallenberg, *Inorg. Chem.*, 1997, **36**, 172-176.
66. C. E. McCusker and F. N. Castellano, *Inorg. Chem.*, 2015, **54**, 6035-6042.